Lagrangian coherent structures and the dynamics of inertial particles

Sudharsan Madhavan

A dissertation
submitted in partial fulfillment of the
requirements for the degree of

Master of Science

University of Washington

2014

Reading Committee:

James J. Riley, Chair

Steven L. Brunton

J. Nathan Kutz

Christopher S. Bretherton

Program Authorized to Offer Degree:
UW Applied Mathematics

University of Washington

Abstract

Lagrangian coherent structures and the dynamics of inertial particles

Sudharsan Madhavan

Chair of the Supervisory Committee:
James J. Riley
Professor, Mechanical Engineering
Adjunct Professor, Applied Mathematics

Dynamics of inertial particles in two-dimensional planar flow have been investigated by evaluating finite-time Lyapunov exponents (FTLE). The first part of our work deals with inertial particle dynamics. The Maxey-Riley equations have been employed to track particles. Patterns formed by inertial particles are reported along with their dependance on Strokes number and density of particles relative to the carrier-fluid density. Our results distinguish patterns formed by particles denser than the fluid (aerosols) from those formed by particles lighter than the fluid (bubbles). Preferential concentration of these particles at specific regions of the flow have been observed. The attenuating, low-pass filter effect of Stokes drag on bubbles are reported for the first time. The results from this part of the work motivated further investigations into the underlying organizing structures of the flow, namely the Lagrangian coherent structures (LCS). LCS is traditionally evaluated using FTLE.

In the next part of the work, our objective was to interpret the dynamics of inertial particles by evaluating finite-time Lyapunov exponents on their trajectories. A main result is that aerosols were found to be attracted and preferentially concentrated along ridges of negative finite-time Lyapunov exponents (nFTLE) of the underlying flow. On the other hand bubbles were found to be repelled from these structures and were therefore observed

preferentially concentrating away from these zones. These results, being reported for the first time, supplement the existing literature on preferential concentration of inertial particles. Despite having an effect on particle trajectories, increasing the Stokes number had very little effect on inertial finite-time Lyapunov exponents (iFTLE). Furthermore, increasing Stokes number resulted in an increase in the ridges of iFTLE contours for aerosols, whereas for bubbles the opposite was observed. These findings indicate that optimum mixing occurs at different Stokes numbers for aerosols and bubbles.

The last part of the work focussed on comparing well-known dispersion measures with inertial finite-time Lyapunov exponents. We qualitatively show that two-point dispersion contours share dominant ridges with those from inertial finite-time Lyapunov exponents. This result numerically shows that material surfaces identified by inertial finite-time Lyapunov exponents are maximally dispersed in the flow. Applications and future directions based on our work are suggested.

TABLE OF CONTENTS

LIST OF FIGURES

ACKNOWLEDGMENTS

I am greatly indebted to my mentors and research advisers James J. Riley and Steven L. Brunton for their guidance and encouraging advises throughout these years. Their constant source of motivation and encouragement has helped me to advance a great deal throughout this project. My respect also extends to the moral support they gave me at various standstill points in research. They have been a constant source of inspiration all along my graduate program. Thanks are also due to the Applied Mathematics department for having provided me Teaching Assistantship opportunities.

The conducive research environment at the UW has introduced me to rigorous research of the present day. I would associate a fair share of the favorable environment to my friends. I thank Arunkumar Byravan for being a close friend to talk with. His easy going attitude along with his culinary skills made my stay in Seattle very pleasurable. I wish to express my thanks to Ramkumar Chokkalingam for being a great friend thoughout. Especially his jests over dinner took me out of school anxiety. Special thanks are also due to Isa K. Thompson for reading Sanskrit alongside, which has become another gleeful passion of mine. Her jovial attitude, bantering comments and philosophical discussions have lowered stress levels and made many of my days.

My acknowledgment will not be complete without showing a major share of my gratefulness to my aunts and my father for both the moral and pecuniary support they provided me with throughout my life. My wholehearted indebtedness is especially due to my aunt for providing me with every possible support during the appalling times of my life.

DEDICATION

This thesis is dedicated to my dear mom, Late Mrs. Parimala Madhavan.

Chapter 1

INTRODUCTION

1.1 Overview of Applications

Poisson [1831] was one of the earliest researchers to work on flow past a rigid sphere. Interestingly he started working on the problem two-decades earlier than the time when Navier-Stokes equations were proposed. In his work he examined the sinusoidal flow past a rigid sphere. His contributions correctly pointed out the added mass effects and its coefficient. In the earlier days his original motivation to study this problem was to predict the motion of a pendulum oscillating in air. Since then, various researchers have worked on accurately predicting the equations of motion of a spherical particle under an uniform flow. Specifically the seminal article Maxey and Riley [1983] and the equations of motion discussed therein clarified the subject. Their article elucidated the work of past researchers with detailed derivations and drew attention to the use of equation for zero Reynolds numbers. These equations of motion being named after the authors as the Maxey-Riley (MR) equations made it easier to study the dynamics of inertial particles in flow. Although other analytic studies extend the MR equations to more general form, the results often involve complicated forms hindering their use in repetitive calculations.

Inertial particle flows are found in abundance both in nature and industrial applications. Consequently the motivation to throughly understand the dynamics of these particles become essential for both fundamental and applied research endeavors. For instance fundamentally they have been studied to answer questions such as "How do inertial particles get dispersed by flow, especially by turbulence ?, How does the inertia of particles affect the gravitational settling velocity and settling time of the particles ?, Why do inertial particles concentrate on specific regions of the flow ?, etc." Applied flows such as inertial particle dispersion by clouds and hurricanes [Shaw et al., 1998, Sapsis and Haller, 2009], oil

spills in the ocean [Beron-Vera et al., 2008, Olascoaga and Haller, 2012, Nencioli et al., 2011, Mezić et al., 2010], urban pollution dispersion [Tang et al., 2012], tracing toxic elements [Natusch et al., 1974], etc., are some of the motivations behind studying the dynamics of inertial particles.

One of the fundamental questions researchers are trying to answer is associated with relative dispersion of inertial particles by turbulence. The idea stems from the fact that dispersion of fluid particles are relatively better known in comparison to those of inertial particles. This is primarily because of the fact that relative dispersion of fluid particles provides us insights into the spatial structure of turbulent flows. Therefore relative dispersion of fluid particles has become a well-studied measure in the last century. However in a significant number of scenarios the particles encountered are inertial in nature. This is because of the very fact that they these particles are different from those of the carrier-fluid. Dispersion of fluid particles by turbulence has been of great interest since the days of G. I. Taylor [Taylor, 1954]. Since then, two-particle fluid dispersion has become a well-studied quantity with great significance in characterizing turbulence. Some notable recent works along these lines include Chen et al. [2006], Biferale et al. [2005], Boffetta and Sokolov [2002], Malik and Vassilicos [1999], Fung and Vassilicos [1998]. Specifically turbulent-like models are usually validated by comparing their two-particle fluid dispersion characteristics with those from direct numerical simulation [Malik and Vassilicos, 1999]. Boffetta and Sokolov [2002] investigated Lagrangian relative dispersion in direct numerical simulation of two-dimensional inverse cascade turbulence. They have demonstrated results in good agreement with Richardson's original description of diffusion. Biferale et al. [2005] performed a detailed investigation of the particle pair separation through homogeneous turbulence. Through their numerical simulation Biferale et al. [2005] presents the process of particle pair separation as a pdf (probability density function) of separation distance and its second order moment. Through the latter they have estimated Richardson's constant, which was found to be in good agreement with the classical theory. For a detailed review of the two-particle dispersion the readers are referred to the excellent review, Salazar and Collins [2009].

Gravitational settling of particles has been an another motivation to study the dynamics of inertial particles [Rubin et al., 1995, Maxey, 1987a,b, Maxey and Corrsin, 1986]. Maxey and Corrsin [1986] computed statistics for the motion of small particles settling under gravity in an ensemble of randomly oriented, cellular flow fields that are steady in time. They have concluded that particles characterized by small free fall velocity and weak inertia show a strong tendency to collect along isolated paths. In a sequel Maxey [1987b] analyzed for first time the trajectories of particles with densities less than that of the carrier-fluid, namely bubbles. Maxey [1987b] also characterized particle trajectories for aerosols, particles with density higher than that of the carrier-fluid. Particle accumulation was found to be a recurring theme for both types of particles. Furthermore Maxey [1987a] showed for the first time that inertial particles dropped in a Gaussian random velocity field get accumulated and are biased in their trajectories towards regions of high strain rate or low vorticity. This bias in the behavior of inertial particles was construed to be a reason for the change in mean settling velocity. The aforesaid phenomenon was termed later as '*preferential concentration*' of inertial particles. Rubin et al. [1995] showed that when inertia is taken as a small parameter the solution to particle motion admits a globally attracting slow manifold. Structure of these set of attracting paths on these manifolds including stability and bifurcation scenarios were reported.

Preferential concentration of particles has spurred interests among researchers, especially preferential concentration in turbulent flows [Chen et al., 2006, Wood et al., 2005, Shaw et al., 1998, Fessler et al., 1994, Eaton and Fessler, 1994, Squires and Eaton, 1991]. Squires and Eaton [1991] performed a direct numerical simulation of isotropic turbulence with 1000000 particles. Particles were assumed to be denser than the carrier-fluid. Their results showed that particles were collected preferentially in regions of low vorticity, high strain rate regions. They had concluded that turbulence may actually be inhibiting mixing between inertial particles, because dense particles collect in regions of low vorticity and high strain rate. For an excellent review on the subject, the readers are referred to Eaton and Fessler [1994]. Eaton and Fessler [1994] summarizes preferential concentration

effects over a wide range of turbulent flows. They point out that preferential concentration is strongest for Stokes numbers near 1. Despite this fact most developed turbulent flows have intense vortical structures spanning a wide range of length scales. Consequently particles may concentrate on different regions depending on their Stokes number. The review closes with a comment on large eddy simulation holding the capacity to model preferential concentration effects. However a caveat on the considerable work required in developing an appropriate sub-grid scale model which would incorporate preferential concentration effect at small scales was pointed out.

1.2 Scope of the present study

As pointed out in Eaton and Fessler [1994] up until now, there has been little recognition on the effect of preferential concentration in practical applications. Also as suggested in the above work, we are convinced that this phenomenon is important. Consequently it is expected to gain more recognition in many applications as suggested by Eaton and Fessler [1994].

The scope of the current study is to apply well established techniques from dynamical systems on the dynamics of inertial particles. We are specifically interested in evaluating the so called 'Lagrangian coherent structures' which will be introduced in the next chapter of this work. In that identifying the zones of preferential concentration accurately has been one of our motives.

1.3 Organization of the thesis

The first chapter deals with the introduction and gives an overview of literature regarding inertial particles. It also provides basis and scope for the work. The second chapter describes and develops the theory behind the tools we borrow from dynamical systems. In addition the second chapter also introduces the Maxey-Riley equations along with a brief treatment about the significance of each term therein. Furthermore a brief treatment on the computational methods employed in the present study is sketched by the end of the sec-

ond chapter. Thus after setting up the necessary background we move on to the chapter on results and discussions. Results dealing with the effect of various parameters on the dynamics of inertial particles are discussed. Additionally the patterns formed by inertial particles are construed with the help of Lagrangian coherent structures. The work culminates with a chapter on conclusion providing a bird-eye view of the significant results from the previous chapter. Along with conclusions, pointers on future directions based on our work are suggested.

Chapter 2

BACKGROUND

2.1 Nature of Lagrangian coherent structures in fluid flows

As early as 1984, Aref demonstrated interest in studying the rich chaotic dynamics (termed '*chaotic advection*') produced as a result of innocent-looking Lagrangian advection equations such as the following.

$$\dot{\mathbf{x}}\left(\mathbf{x_0},\ t_0,\ t\right)\ =\ \mathbf{u}\left(\mathbf{x},\ t\right). \tag{2.1}$$

More recent developments have led us to understand the dynamics better than the simple description from eq. 2.1. We will outline some of the ideas that have motivated researchers from fluid dynamics to borrow methods established in chaos theory, such as Lyapunov exponents. Equation 2.1 is an ODE (ordinary differential equation) that could be analyzed in detail at least for two dimensional steady flows (autonomous) using tools from dynamical systems. It is known that hyperbolic fixed points and their corresponding stable and unstable manifolds organize the entire flow for such an autonomous system. In this context, flow refers to the solution to the continuous-time dynamical system eq. 2.1, rather than the fluid flow. Therefore, at least in autonomous systems the set of hyperbolic fixed points and their stable and unstable manifolds behave as *separatrices*, organizing the entire flow. A separatrix is more general trajectory in the phase plane that delineates a boundary between trajectories of dynamically distinct characteristics. However if the system considered is 3 dimensional and/or the system is non-autonomous (unsteady) then, even the notion of separatrices becomes difficult to comprehend. For instance, a hyperbolic fixed point of an non-autonomous system can change its stability with time, therefore even the notion of stable and unstable manifolds becomes vague in these systems.

In order to extend the classical techniques of dynamical systems, firstly consider the

simplest extension one can make to the two dimensional autonomous (steady) system is by making the system into a periodic, non-autonomous one. This can be easily achieved by adding a periodic perturbation (dependent on time) to the original autonomous system. This perturbation can give rise to rich dynamics, which may lead to chaos. In these systems, as one might expect, instead of hyperbolic fixed points and their manifolds organizing the flow, a moving material surface takes up this role. Since the system is periodic, Poincar$\acute{e}$ maps in time becomes an important tool in revealing the periodic orbits. A systematic investigation such as the one described above was performed in Rom-Kedar et al. [1990] on periodic non-autonomous systems. In order to develop better intuition about Lagrangian coherent structures, we will briefly look at the system from Rom-Kedar et al. [1990]. They examined the flow governed by a pair of vortices under the influence of an external strain-rate field.

$$\psi \;=\; -\frac{\Gamma}{4\pi}\log\left[\frac{(x-x_v)^2+(y-y_v)^2}{(x-x_v)^2+(y+y_v)^2}\right] - V_v y + \epsilon x y \sin(\omega t)\,, \tag{2.2}$$

Where ψ is stream function of the flow in a frame moving with the average velocity of the vortices. $\pm\Gamma$ represents the circulations of the vortices. ϵ denotes the strain rate while V_v is the average velocity of the vortex pair. The vortices are separated by a distance $2d$ in the y-direction with $(x_v(t),\ \pm\, y_v(t))$ representing their positions.

The above system 2.2 resembling a vortex pair and a periodic perturbation was con-

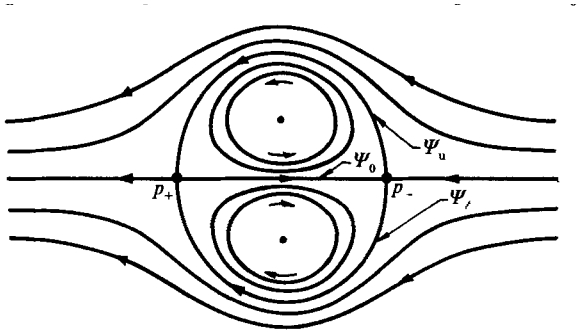

Figure 2.1: Streamlines of unperturbed flow obtained by setting $\epsilon = 0$ from eq. 2.2 from Rom-Kedar et al. [1990].

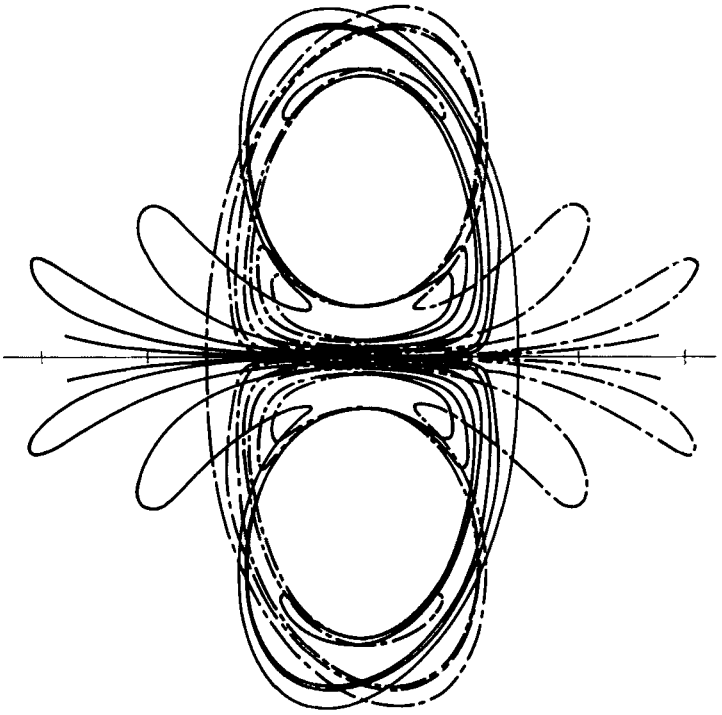

Figure 2.2: Homoclinic tangle of system 2.2. ———, unstable manifold; —.—.— , stable manifold, from Rom-Kedar et al. [1990].

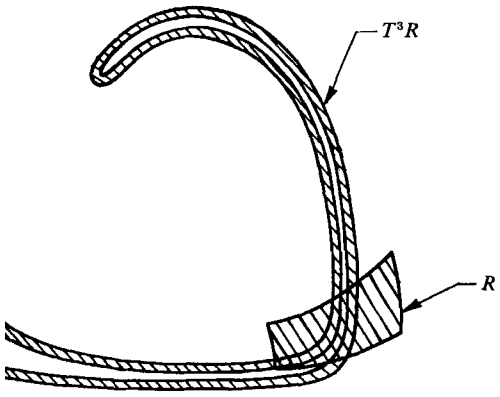

Figure 2.3: Horseshoe, from Rom-Kedar et al. [1990].

sidered by Rom-Kedar et al. [1990]. The corresponding unperturbed system (obtained by setting $\epsilon = 0$) is shown in fig. 2.1. In fig. 2.1 the stagnation points p_- and p_+ denote the fixed points of the autonomous system given in 2.2. From the figure, it can be seen that particles initiated on Ψ_u or Ψ_l asymptotically reach p_+ when integrated forward in time. On the other hand, integrating backwards in time, they reach p_-, therefore Ψ_u and Ψ_l are subsets of the stable and unstable manifolds of p_+ and p_- respectively. Similarly, Ψ_0 is part of the stable and unstable manifold of p_- and p_+ respectively. Notice that, in the unperturbed system, the stable and unstable manifolds coincide with the streamlines of the flow. However such a simple representation does not hold as soon as the system is periodically perturbed. The stable and unstable manifolds in the perturbed scenario for sufficiently small perturbations are smooth invariant curves from the unperturbed system. In fact, perturbing the system according to 2.2 results in a homoclinic tangle as shown in fig. 2.2, supporting chaos in particle trajectories. Moreover Rom-Kedar et al. [1990] also analytically proves the existence of a horseshoe map, as shown in fig. 2.3, thus unequivocally establishing chaos in particle trajectories. The emphasis in presenting these results is to show that neat[1] heteroclinic connections in the autonomous (steady) system has changed into a complicated homoclinic tangle with the addition of periodic perturbations.

However flows encountered in industrial applications or natural phenomena are more complicated, especially since they are not necessarily representable as periodic perturbations to an autonomous system[2]. One might like to extend these type of analyses to such general systems. However even some of the definitions[3] are not clear for such systems. Consequently, we would want to adopt a less restrictive and more general approach to comprehend transport in such general systems.

One such notion is the usage of LCS (Lagrangian Coherent Structures) Haller and Yuan [2000]. They are Lagrangian in the sense that the structures we compute are those moving along with the fluid and they are coherent because of their distinguished stability prop-

---

[1]Implying lesser mixing between fluid particles.

[2]Consider for example flow past bluff bodies, fluid instabilities of various kinds, mixing problems from atmosphic and oceanic flows.

[3]For instance stable and unstable manifolds.

erties (strongest locally attracting/repelling material surfaces). For instance some visualization studies such as the one shown in fig. 2.6 were successful in identifying structures resembling LCS. With the stability based notion aforesaid, one can think of LCS as an analogous quantity to unstable manifolds of an autonomous (steady) system.

However, the computational methodology to estimate them based on the notion of

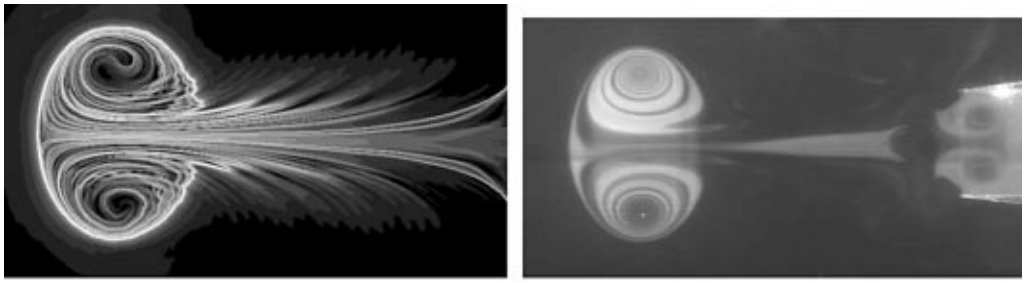

Figure 2.4: Comparison of LCS (panel a) with experimental florescence visualization (panel b) by Paul S. Krueger and John O. Dabiri (as cited in Shadden [2005]), illustrating distinguished stability properties of LCS.

stability is not clear. First of all, it is surprising to note that trajectories hyperbolic at an instant may change *stability* at another instant. Furthermore, defining stable and unstable manifolds require precise asymptotic limit sets. However the data available about the flow fields are only finite (be it experimental or numerical). Therefore notions such as the stable manifolds/unstable manifolds are less clearly defined and less amenable to analysis. But as we said earlier we want to implement a less restrictive, and a more general approach. The central idea is the fact that any trajectory may lose or gain hyperbolicity over time Haller and Poje [1998], and one wishes to compute these surfaces by evaluating surfaces for this property. However evaluating such a criteria on every possible material surface in the domain is impossible since there are infinitely many such possible surfaces.

On the other hand, a global approach that measures Lagrangian expansion rate would be a better method to employ. LCS are traditionally evaluated via the Lagrangian measure named finite time Lyapunov exponents (FTLE). We start by discretizing the fluid domain

with a dense grid observe the Lagrangian expansion rate and extract FTLE to obtain repelling LCS. In order to get attracting LCS, we would simply reverse time since expansion in forward time would mean contractions in reverse time and vise-versa.

We are now ready to define FTLE.

Consider a set of fluid particles in a flow advected by the Lagrange equation as given by eq. 2.1. Assuming a pair of arbitrary material points (located at x_0 and $x_0 + \xi_0$ at $t = 0$) and modeling Lagrangian expansion rate for a pair of particles with initial separation of ξ_0,

$$|\xi_t| \approx e^{\Lambda(t-t_0)} \quad |\xi_0|$$

(or)

$$\frac{|\xi_t|}{|\xi_0|} \approx e^{\Lambda(t-t_0)}, \tag{2.3}$$

Where Λ is defined to be the FTLE. Now, an alternate expression for ξ_t can be derived by considering the flow map, $F_{t_0}^t$ which maps points from $\mathbf{x_0}$ at t_0 to their corresponding positions at t, namely, $\mathbf{x}$, as given below.

$$F_{t_0}^t \; : \; \mathbf{x_0} \; \mapsto \; \mathbf{x}\left(\mathbf{x_0},\; t_0,\; t\right).$$

Therefore ξ_t can be written in terms of $F_{t_0}^t$ as follows,

$$\xi_t \; = \; F_{t_0}^t\left(x_0 \; + \; \xi_0\right) \; - \; F_{t_0}^t\left(x_0\right). \tag{2.4}$$

This motivates us to expand $F_{t_0}^t\left(x_0 \; + \; \xi_0\right)$ in terms of ξ_0, the initial separation between the pair of material points, as below,

$$|\xi_t| \; = \; \left|\nabla F_{t_0}^t\left(x_0\right) \; \cdot \; \xi_0\right| \; + \; \mathcal{O}\left(|\xi_0|^2\right).$$

Using the Euclidean norm to represent the above quantity,

$$|\xi_t| \; = \; \sqrt{e^T \cdot \; \nabla F_{t_0}^t\left(x_0\right)^T \; \cdot \; \nabla F_{t_0}^t\left(x_0\right) \; \cdot \; e} \; |\xi_0| \; + \mathcal{O}\left(|\xi_0|^2\right), \tag{2.5}$$

With $(\bullet)^T$ representing the transpose of $(\bullet)$ and $e = \xi_0/|\xi_o|$, therefore in the limit as $|\xi_0| \to 0$,

$$\lim_{|\xi_0| \to 0} \frac{|\xi_t|}{|\xi_0|} \;=\; \sqrt{e^T \cdot \nabla F_{t_0}^t \left(x_0\right)^T \cdot \nabla F_{t_0}^t \left(x_0\right) \cdot e}\,. \tag{2.6}$$

Now consider the definition,

$$\mathbf{C}(x_0, t_0, t) \;=\; \nabla F_{t_0}^t \left(x_0\right)^T \cdot \nabla F_{t_0}^t \left(x_0\right), \tag{2.7}$$

where $\mathbf{C}$ in eq. 2.7 is the right Cauchy – Green strain tensor. Let, $\lambda^i(x_0, t_0, t)$ denote the i^{th} eigenvalue of $\mathbf{C}$ numbered in decreasing order, and e^i be the associated eigenvector. Then expanding in this direction gives,

$$\lim_{|\xi_0| \to 0} \frac{|\xi_t|}{|\xi_0|} = \sqrt{\lambda^i(x_0, t_0, t)}.$$

Also it is noteworthy that $\sqrt{\lambda^i} \;=\; \sigma^i$ is the singular value of deformation gradient, $\nabla F_{t_0}^t \left(x_0\right)$. Now consider the definition of FTLE as averaged over the integration time and after applying natural logarithms as below,

$$\Lambda^i \left(x_0,\; t_0,\; t\right) \;=\; \frac{1}{|t - t_0|} \;\ln\left(\sqrt{\lambda^i \left(x_0,\; t_0,\; t\right)}\right) \;=\; \frac{1}{|t - t_0|} \;\ln\left(\sigma^i \left(x_0,\; t_0,\; t\right)\right). \tag{2.8}$$

From the above definition of Λ, the FTLE is clearly a function of space, time and integration length. Note that geometrical features of Λ, λ, σ are roughly equivalent. However, Λ, the FTLE as defined above is also maximal along trajectories of high shear. Remembering the definition of hyperbolicity[4], we want to eliminate these shear structures from our ridges of FTLE. For instance consider the system define by eq. 2.5. An illustration of such a shear type flow is given in fig. 2.5 (b).

$$\dot{x} \;=\; 2 + \tanh(y), \tag{2.9a}$$

$$\dot{y} \;=\; 0, \tag{2.9b}$$

[4]We want to capture saddle type separations and isolate simple shear ones, which do not constitute LCS.

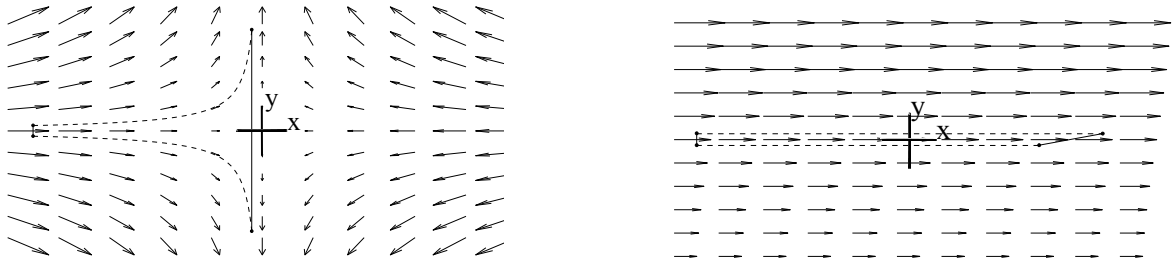

(a) Saddle flow (b) Shear flow

Figure 2.5: Saddle like flow (a) vs shear dominated flow (b) illustration adapted from Shadden [2005].

In fig. 2.5 FTLE, in addition to being maximized along saddle type separations, are also maximal along the shear flow as found in fig. 2.5 (b). Consequently our current definition of FTLE would produce an ridge along fig. 2.5 (b). There are a number of ways to deal with this problem. A very brief discussion on some of them are below. We could apply the definition of hyperbolically as below. Integrating a set of close enough set of particles on the surface should exhibit saddle type behavior at least locally. Based on this Haller [2011] derives a necessary and sufficient criteria to filter out the shear dominated ridges. There are also other intuitive methods such as requiring the FTLE fields to be objective. A quantity in this context is called objective if it remains invariant under translations and rotations. Since Λ is a relative measure, they remain objective under suitable transformations.

Before we begin to compute these structures, let us look at an application to get an idea about the results they can give us. The following fig. 2.6 represents the FTLE computation on a experimentally generated vortex ring. Notice that the traditional Eulerian measures such as vector fields don't reveal much information on fluid entrainment and vortex boundaries as shown. Of late this information is believed to be an essential part for understanding transport and to devise effective control strategies.

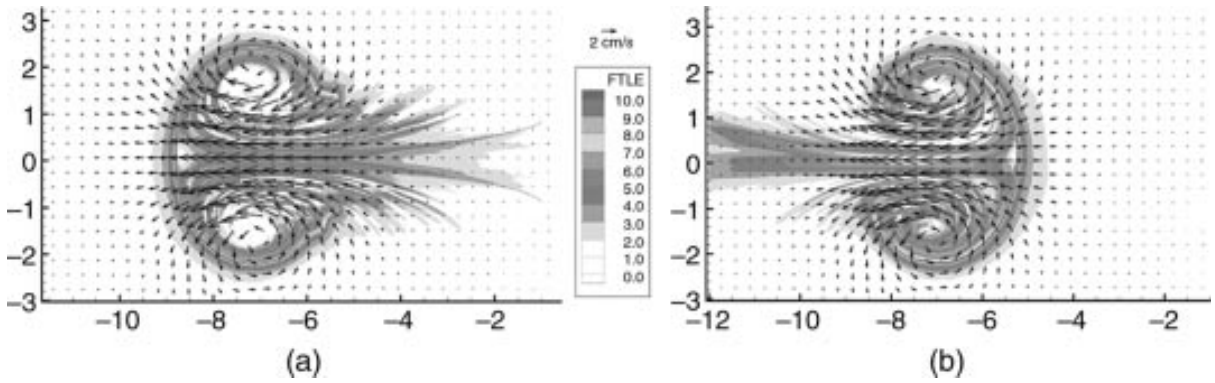

Figure 2.6: Empirical vortex ring reveal attracting/repelling LCS that define the vortex boundary, transport and mixing. [Shadden, 2005, Shadden et al., 2007]

2.2 Basics of inertial particles in flows

Up to this point we have assumed the particles behave much like those of the underlying fluid, i.e., advected particles always follow the flow to which they are subjected. However we could repeat the same analysis on various derived quantities of $\dot{\mathbf{x}}$, the velocity fields. In particular it is interesting to see the conclusions if the particles we integrate are particles of finite size and with densities different from that of the fluid. We can do this if we could track inertial particles with good accuracy. In order to track such particles, we employ the results from the seminal article, Maxey and Riley [1983], named Maxey-Riley equations. Assuming $r(t)$ to represent the position of a particle at time t and $v(t) = \dot{r(t)}$ to represent the corresponding velocity of the particle then, the dimensional form of the equations are as given by eq 2.10.

$$\begin{aligned} m_p\,\dot{v} \;=\; m_f\,\frac{d}{dt}u\left(r\left(t\right),t\right) \;-\; \frac{1}{2}m_f\,\frac{d}{dt}\left(v-u\left(r\left(t\right),t\right) \;-\; \frac{1}{10}a^2\nabla^2 u\left(r\left(t\right),t\right)\right) \\ -\,6\pi a\mu X\left(t\right)+\left(m_p-m_f\right)g-6\pi a^2\mu\int_0^t d\tau\;\frac{\frac{dX(\tau)}{d\tau}}{\sqrt{\pi\nu\left(t-\tau\right)}}, \end{aligned} \tag{2.10}$$

with

$$X(t) \;=\; v(t) \;-\; u(r(t),\, t) \;-\; \frac{1}{6}a^2\nabla^2 u$$

Here m_p is mass of the inertial particle, m_f is mass of the fluid displaced by the particle, $u(r(t), t)$ represents the velocity of fluid particle at the location $r(t)$ and time t, μ represents the viscosity of the underlying fluid, a represents the radius of the particle and g represents the acceleration due to gravity. Here, the derivative $du/dt = \partial u/\partial t + (u.\nabla)u$ is the total derivative defined in the usual notations.

The first term in eq. 2.10 amounts for the force exerted by undisturbed fluid on the particle, while the second the term accounts for the added mass effects due the underlying fluid. Third and fourth terms constitute Stokes drag and buoyancy effects respectively. The integral term is called as the Basset history term accounting for the effect of particle modifying the flow gradients locally. The $a^2\nabla^2 u$ term is named as the Faxen correction, performed to justify nonuniform flow effects encountered by the inertial particle.

Equation 2.10 is valid for small spherical, rigid particles with low particle Reynolds numbers, i.e., Reynolds number computed using the particle radius, a as the length scale. Assuming sufficiently small particle radius, a, Faxen correction terms can be neglected. The Basset history term can also be neglected assuming that particle's time interval to revisit a region it has visited earlier is large in comparison to the time scale of the problem. Non-dimensionalizing eq. 2.10 using the time scale and the length scale of the flow yields eq. 2.11.

$$\ddot{r}(t) \;=\; \frac{1}{\mathrm{St}}\;(u(r(t),t) - \dot{r}(t)) \;-\; W\cdot n \;+\; \frac{3}{2}R\,\frac{d}{dt}u(r(t),t)\,, \tag{2.11}$$

Where

$$\mathrm{St}^{-1} \;=\; \frac{6\pi a\mu L}{\left(m_p + \frac{1}{2}m_F\right)U}, \qquad R \;=\; \frac{m_f}{m_p + \frac{1}{2}m_f}\,, \qquad W \;=\; \frac{m_p \;-\; m_f}{6\pi\; a\mu U\;\mathrm{St}}\;g,$$

n is unit vector pointing in the direction of gravity. Furthermore gravity is not considered throughout this work for the sake of simplicity. As a result, eq 2.11 reduces to eq. 2.12 with

two non-dimensional quantities characterizing the physical properties of the particle.

$$\ddot{r}\left(t\right) \;=\; \frac{1}{\mathrm{St}}\;\left(u\left(r\left(t\right),t\right) \;-\; \dot{r}\left(t\right)\right) + \;\frac{3}{2}R\;\frac{d}{dt}u\left(r\left(t\right),t\right), \tag{2.12}$$

Where St is the Stokes number defined as the ratio of the characteristic time of a particle (or droplet) to a characteristic time of the flow. $St \to 0$ implies particles behaving closer to that of the flow. On the other hand higher St particles tend to deviate from fluid trajectories. R is the density ratio parameter. Notice that with $R = \frac{2}{3}$ the particles have the same density as that of the carrier-fluid. If $R > \frac{2}{3}$ then the particles are lighter than the carrier-fluid. Similarly particles with $R < \frac{2}{3}$ are denser than the carrier-fluid and are appropriately called as the aerosols.

It is noteworthy that particles with same density as that of the carrier-fluid ($R = \frac{2}{3}$) and initiated with $\dot{r}(0) = u(r(0), 0)$, track the fluid particles, ie., $\dot{r}(r(t), t) = u(r(t), t)$ and $r(t) = \int_0^t u(\tau)d\tau + r(0)$.

2.3 Computational methodology

In order to compute inertial FTLE (iFTLE) we integrate a set of particles starting out on a uniform grid using eq 2.10 from an initial time, t_0 (say) to a final time, t_f. For instance consider an array of particles initiated at $r_{ij}(t_o)$. Since the particles are inertial, we integrate the system of differential equations as below.

$$\ddot{r}\left(t\right) \;=\; \frac{1}{\mathrm{St}}\;\left(u\left(r\left(t\right),t\right) \;-\; \dot{r}\left(t\right)\right) + \;\frac{3}{2}R\;\frac{d}{dt}u\left(r\left(t\right),t\right), \tag{2.12 revisited}$$

$$r(t) = \int_{t_o}^{t_f} \dot{r}(\tau)d\tau + r(t_0). \tag{2.13}$$

Sufficient accuracy and smoothness are essential to solve the above system numerically since we ultimately want to measure exponential growth in trajectories. Therefore care has been taken to employ sufficiently small time stepping with a 4th order Runge-Kutta integrator to integrate the system 3.3. Once the position of particles are known, the defor-

mation gradient, $\nabla F_{t_0}^t(x_0)$, can be computed. FTLE can be then calculated at each location by evaluating the largest singular value of the corresponding deformation gradient matrix. Since FTLE from the above strategy are computed from $\nabla F_{t_0}^t(x_0)$ and plotted at x_0, new release and tracking of an uniform grid of particles are required for each time instance considered.

Chapter 3

RESULTS AND DISCUSSIONS

Numerical integration of uniformly spaced particles according to the MR equations [Maxey and Riley, 1983, Tél et al., 2005] and computation of Finite time Lyapunov exponents (FTLE) on their trajectories following the approach detailed in section 2.3 are now carried out for particles varying in St and R. In particular, particles ranging from fluid particles ($St = 0.01$) to those with relatively large inertia ($St = 2$), were considered by varying St. Furthermore, the mass of the particles was altered by changing the non-dimensional number R, with $R < \frac{2}{3}$ denoting aerosol-like particles with densities higher than that of the carrier-fluid and $R > \frac{2}{3}$ denoting bubble-like particles with densities lower than that of the carrier-fluid. Additionally, the effect of base flow frequency, ω on these particle trajectories are also considered.

3.1 Dynamics of inertial particles

3.1.1 Effect of Stokes number

It is well-known that inertial particles possess more degrees of freedom, than fluid particles i.e., assuming planar incompressible flow, the inertial particles system is four dimensional, (x, y, v_x, v_y)[1] whereas that of the non-inertial particles consists of only two dimensions, (x, y). This is due to the fact that inertial particles are non-constrained by incompressibility, hence v_x, v_y can be different from the local fluid velocities.

In light of this argument it appears as if inertial particles will continue to possess extra degrees of freedom. However, the inertial dynamics are monotonically dissipative as opposed to non-inertial flows where the phase space (x, y) is preserved. Consequently in

[1]Here $(x, y, v_x, v_y) = (\overrightarrow{r}, \overrightarrow{\dot{r}})$.

due course, the dimensionality of an inertial dynamical system is guaranteed to fall short of that of a non-inertial one. Given the fact that the dimensionality of inertial systems decreases monotonically over time, it is natural to expect fractional dimensionality in these systems. It follows that these structures show up as fractal structures on the projected two dimensional (x, y) phase space. In fact it is not uncommon to encounter strange and chaotic attractor dynamics. Readers are refereed to Tél et al. [2005] for an excellent review on related phenomena.

In order to first visualize the dissipative nature of phase space, we will make use of the flow defined by the double gyre stream-function given below.

$$\psi\,(x,\ y,\ t)\ =\ A\ \sin\ (\pi\ f\,(x,\ t))\ \sin\ (\pi y)\,, \tag{3.1}$$

where

$$f\ (x,\ t)\ =\ a\,(t)\ x^2\ +\ b\,(t)\ x, \tag{3.2a}$$

$$a\,(t)\ =\ \epsilon\ \sin\ (\omega t)\,, \tag{3.2b}$$

$$b\,(t)\ =\ 1-2\epsilon\ \sin\ (\omega t)\,. \tag{3.2c}$$

We consider the double-gyre system defined above over the suitable rectangular domain, [0, 2] x [0, 1]. As seen from the equations, the stream function is a combination of sinusoidal composite functions. Specifically the quadratic function $f(x,\ t)$ leads to periodic oscillations across the domain. Consequently the double gyre system consists of a pair of vortices oscillating back and forth within the cell, [0, 2] x [0, 1]. In fact setting $\omega\ =\ 0$ results in a steady flow field with a pair of vortices centered at $(0.5, 0.5)$ and $(1.5, 0.5)$. Also, it is noteworthy that any two dimensional planar system defined by a stream function is a Hamiltonian system with its Hamiltonian being the scalar stream function, ψ. Therefore the conjugate and momentum coordinate pair relation with the Hamiltonian holds. In other words, the phase space (x, y) is conserved in accordance with incompressibility of flows:

$$\dot{x} = \frac{\partial \psi}{\partial y}, \tag{3.3a}$$

$$\dot{y} = -\frac{\partial \psi}{\partial x}. \tag{3.3b}$$

In the following analysis, we increase the Stokes number of the particles and advect them on the double gyre flow. Stokes number, $St = \frac{\left(m_p + \frac{1}{2} m_F\right) U}{6\pi a \mu L}$, represents the non-dimensional particle response time relative to the hydrodynamic time scale of the flow. For instance, one would expect that for low St, ideally $St \to 0$ inertial particles to behave similar to the fluid particles. As St is increased, we would expect inertial particles to respond poorly to flow changes. A consequence of the aforesaid statement is illustrated in Fig. 3.1. We see aerosol ($R = 0$) particles with $St = 0.1$ to be more phase space filling and therefore relatively more closely following non-inertial particles than their counterpart with higher Stokes number. Similar patterns are also observed with increase in St for bubble-like particles ($R = 1$). Moreover as mentioned earlier inertial particles, being not constrained by incompressibility, start with more degrees of freedom and dimensionality. However because of dissipative nature of the Stokes drag term, the phase space of inertial particles decrease monotonically in time. As a result we see that with increase in St, the projection of the phase space onto phase space, ($x,\ y$) contracts faster, resulting in increasingly thin structures each with dimensionality less than two.

3.1.2 Effect of inertia of particles

Fig. 3.2 compares particle trajectories for various St and R. In general particles with $St \ll 1$ would respond faster to the underlying flow, thereby exhibiting near incompressibility. For instance Fig. 3.2 (a) & (c) show no noticeable change in comparison to Fig. 3.2 (b) (neutrally buoyant) while Fig. 3.2 (g) & (i) significantly differ from their counterpart Fig. 3.2 (h). As St is increased, the particle response time to flow time is increased. Therefore we would expect the particles to respond more poorly to the flow. In addition as St is increased par-

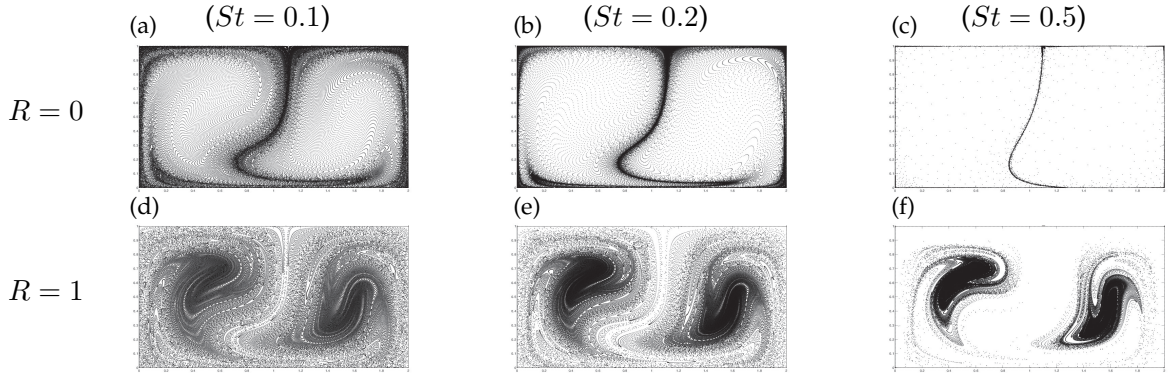

Figure 3.1: Patterns formed by particles of various St advected from a set of uniformly distributed particles at $t = 15, \omega = \frac{6\pi}{10}$.

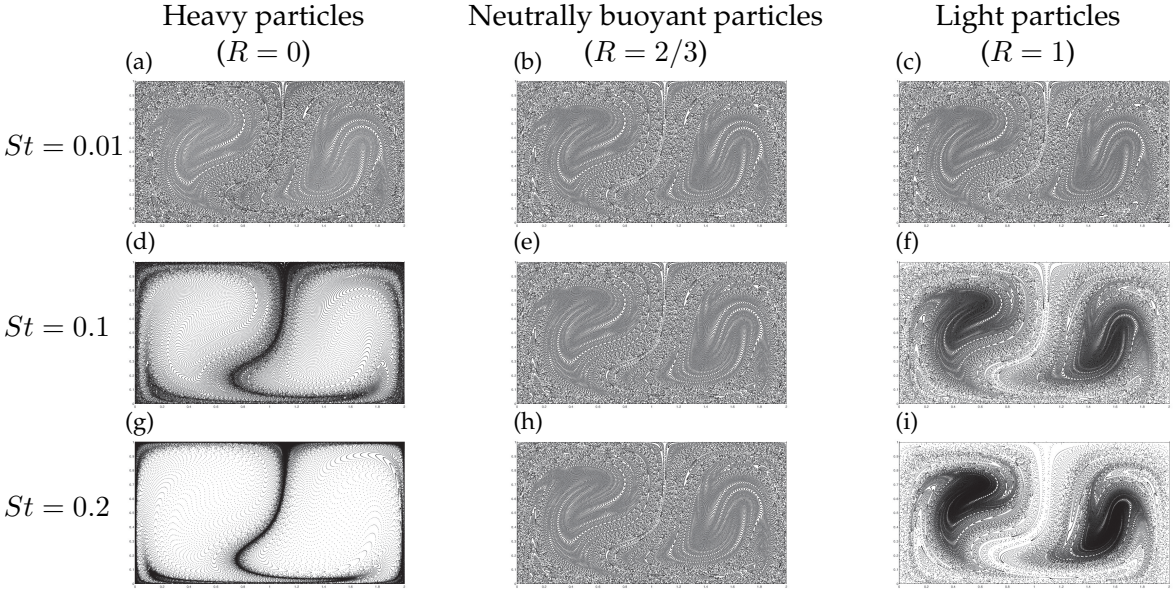

Figure 3.2: Inertial particles integrated on $\omega = \frac{2\pi}{10}$ Doublegyre flow until $t = 15$.

ticles tend to dissipate (x, y) phase space at a faster rate. This effect is clearly seen in fig. 3.2 (d), (f), (g) & (i). However as pointed earlier, it can be shown that neutrally buoyant particles ($R = \frac{2}{3}$) initiated with local flow velocity, follow the corresponding fluid particles,

i.e., $v(t) = u(t)$. As a consequence there is no significant change after increasing St for neutrally buoyant particles.

Moreover increasing the inertial term R in equation 2.12 results in particles preferentially concentrating on certain regions of the flow. Specifically $R = 0$, aerosol particles are centrifuged out of the vortex cores and are found preferentially concentrating in the low vorticity, high rate of strain regions, while $R = 1$, bubbles are concentrated closer to the vorticity cores of the flow. This is primarily because of the variations in the added mass, centrifugal and pressure gradient forces acting on different particles. Specifically an aerosol particle experiences more centrifugal force acting radially outwards from the center of vortices, compared to the pressure gradient force acting radially inwards. Therefore these particles are pushed away from the vorticity cores. On the other hand, a bubble particle with density lesser than the fluid, experiences a stronger pressure gradient force acting radially inwards towards the low pressure, high vorticity regions. Figure 3.2 illustrates this phenomenon of preferential concentration of inertial particles. For instance in Figure 3.2 (d), aerosol particles are concentrated away from the center of vortices while in Figure 3.2 (f) bubble particles are attracted onto the instantaneous centers of vorticity. This effect is more pronounced between Figure 3.2 (g) and (i).

3.1.3 Effect of flow frequency

The double gyre base flow in Eqn. 3.1 has a characteristic frequency ω associated with it. Increasing ω in Eqn. 3.1 results in a corresponding increase in the frequency of oscillation the gyre undergoes. As pointed out earlier, $\omega = 0$ corresponds to steady flow with a pair of steady vortices in $[0, 2]$ x $[0, 1]$.

Consequently we see structures along these vortices in fig. 3.3 (a) & (b). The effect of inertia, as explained in the previous section, can also be observed in fig. 3.3; i.e., for $R = 0$, aerosol particles are attracted onto and hence conglomerating away from the center of vortices in fig. 3.3 (a), while at $R = 1$, the bubble-like particles are drawn into the cores of

vortices as shown in fig. 3.3 (b). In addition to inertial effects, low-pass filter relation of St to position of particles as reported in Bec et al. [2006] is demonstrated in fig. 3.3. For instance, conglomeration of particles along the steady pair of vortices with $\omega = 0$ seen in fig. 3.3 (a) gets distorted into fig. 3.3 (c) when ω is increased to $\frac{6\pi}{10}$. However when ω is further increased by an order of magnitude to 10 as shown in fig. 3.3 (e), inertial particles respond slowly to the relatively high frequency of the flow and as a result reacquire the original structure similar to fig. 3.3 (a). Bec et al. [2006] shows a similar phenomenon in homogenous, isotropic, fully developed turbulent flow. However their work only considered aerosol like particles, $R = 0$. Our results numerically extend these observations to bubble like particles with $R = 1$.

3.2 Finite time Lyapunov exponents

Flow visualization is perhaps the most intuitive and widely employed method to understand fluid mechanics. One of the objectives of flow visualization is to reveal coherent features of the flow by initiating passive neutrally buoyant tracer particles at suitable locations. It is now known that attractive LCS are highlighted in flow visualization studies because of their very definition (see Figure 2.6 and subsequent discussions). Therefore these structures are easier to interpret than repelling LCS and aid us in understanding the flow. However their counterpart, namely, repelling LCS, which can be computed using FTLE, are not visible in flow visualization. The fact that our data driven method to evaluate FTLE can identify such complimentary coherent features of a flow is one of the significant contributions of LCS. In this section we numerically demonstrate the relationship between nFTLE and the preferential concentration of inertial particles, thereby supplementing the existing literature on preferential concentration of inertial particles. Specific distinctions between aerosol-like particles, $R = 0$ and bubble-like particles, $R = 1$ are emphasized.

Inertial FTLEs (iFTLEs) were evaluated on the trajectories of particles as described in Section 2.3. In this section iFTLEs are used as a supplement to interpret particle trajectories.

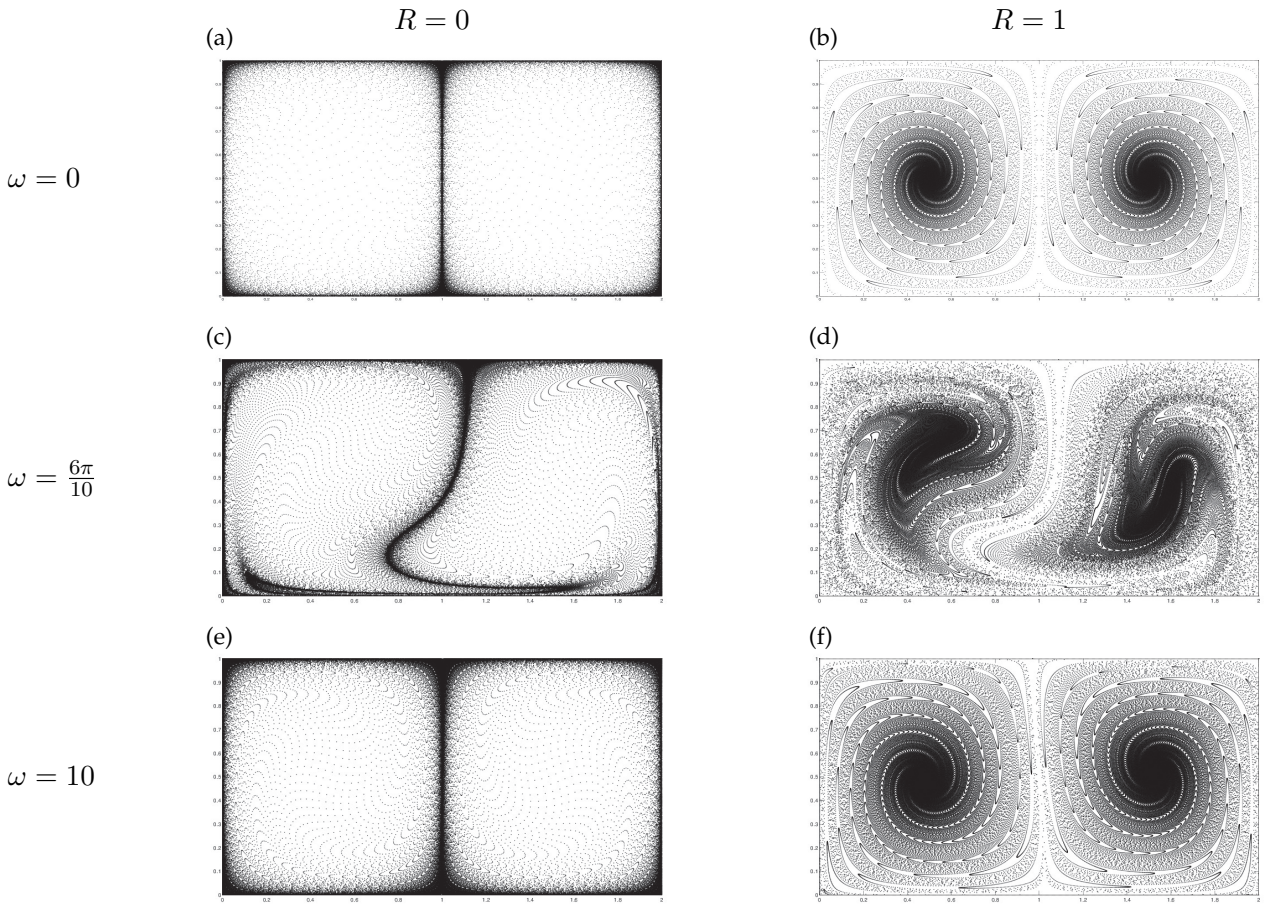

Figure 3.3: Inertial trajectories of particles with $St = 0.2$ illustrating the (lowpass filter type) effect of St on the frequency of the flow.

Specifically preferential concentration of inertial particles are understood using iFTLE.

Figure 3.4 (b) (e) & (h) (red contours) numerically visualize the attracting manifolds of fluid particles, i.e., they were obtained by integrating eq. 2.1 and are therefore non-inertial, fluid tracers. Furthermore in order to visualize attractive structures, we reverse the direction of integration. In other words nFTLE were evaluated on non-inertial flow maps integrated backwards in time, $\Phi^0_{7.5}, \Phi^0_{15}, \Phi^0_{22.5}$ as shown. Ridges of nFTLE represent exponential stretching of fluid particles when integrated backwards in time. Therefore when

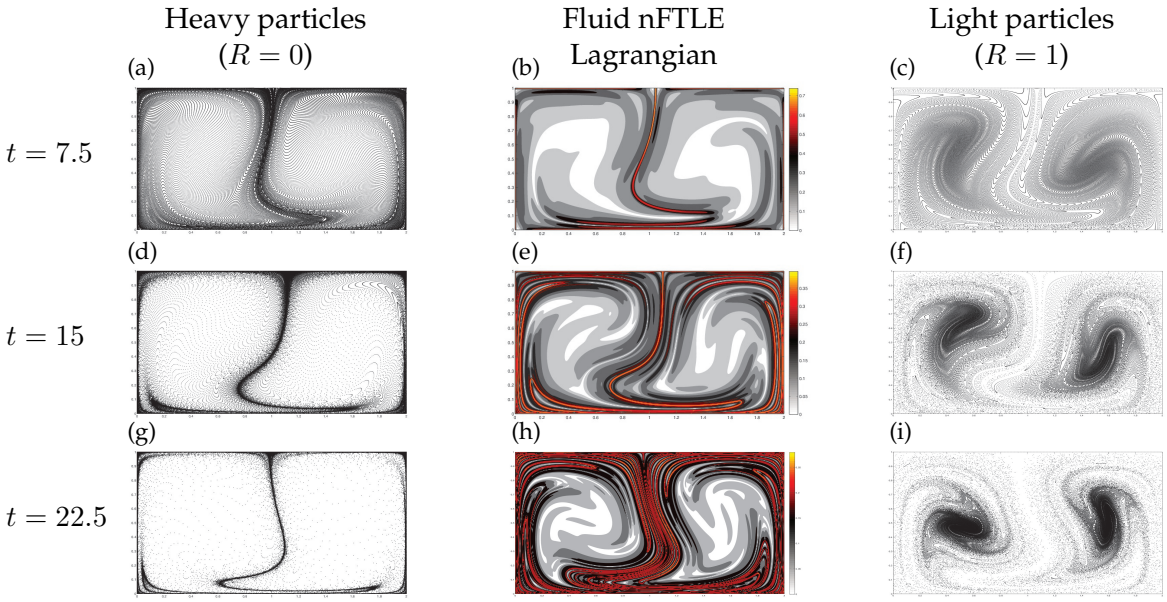

Figure 3.4: Aerosols ($R = 0$) and bubbles ($R = 1$) advected according to the Maxey-Riley equations from an initial uniform distribution (black dots). Attracting manifolds of the underlying fluid particles are visualized by computing Finite time Lyapunov exponents on flow maps $\Phi^0_{7.5}, \Phi^0_{15}, \Phi^0_{22.5}$ (backward integrated) for (b), (e), (h) correspondingly (red contours). Other parameters are $\omega = \frac{6\pi}{10}$, $St = 0.2$, $\epsilon = 0.25$, $A = 0.1$.

fluid particles are advected forward in time, these ridges act as attractive material lines. Its also noteworthy that fig. 3.4 (h) shows relatively more ridges. This indicates higher mixing between particles initiated at the proximity of the ridges since fluid particles do not leave the cell $[0, 2]$ x $[0, 1]$.

Figure 3.4 (a), (d), (g) shows aerosol ($R = 0$) particle trajectories at various times. Similarly fig. 3.4 (c), (f), (i) represent bubble ($R = 1$) trajectories advected forward in time. It is well-known that inertial particles preferentially concentrate depending on their inertia (see Section 3.1.2), i.e., preferential concentration effects provide a rough estimate of particle trajectories based on the local vorticity and the inertia of the particles. However, nFTLE of the underlying fluid system pinpoints these zones more accurately. Thus, they act as a skeleton for aerosol ($R = 0$) attractive manifolds as shown by a striking resemblance

between fig. 3.4 (a), (d), (g) and fig. 3.4 (b), (e), (h) respectively. Therefore, material lines identified by FTLE qualify particle trajectories indicated by classical preferential concentration theories, thereby supplementing existing literature. While aerosol ($R = 0$) particles attract onto the attractive manifolds of the fluids, bubble ($R = 1$) particles are repelled from the same. This can partly be explained by preferential concentration effects. However material lines of nFTLE accurately pinpoint and reveal these structures. These results are suggestive of employing aerosol-like particles with R slightly less than $\frac{2}{3}$ to visualize attractive manifolds, the visible coherent features of the flow. Although neutrally buoyant particles are preferred in flow visualization studies for the purpose of not altering the flow, our results indicate that slightly denser particles with R slightly greater than $\frac{2}{3}$ get organized faster in accordance with the underlying attractive LCS and can therefore be of use in highlighting the coherent structures of the flow.

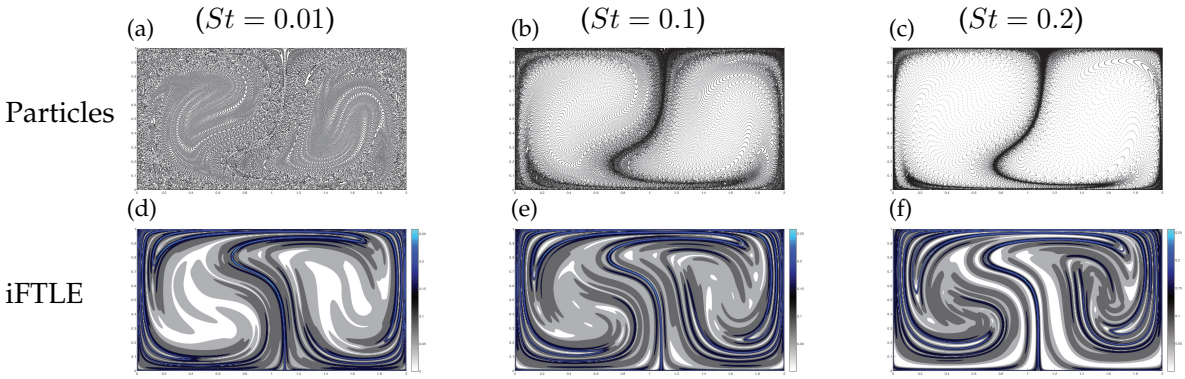

Figure 3.5: Inertial particle trajectories and corresponding iFTLE for various St, other parameters are $t = 15, \omega = \frac{6\pi}{10}$.

Figures 3.5 (a), (b) & (c) show aerosol ($R = 0$) particle positions at $t = 15$ for St varying from 0.01 where particles are behaving closer to fluids to 0.2 where significant dissipation of phase space ($x,\ y$) is characteristic. Their corresponding iFTLE are shown in fig. 3.5 (d), (e) & (f). Since these are computed using the respective forward integrated flow maps, Φ_0^{15}, the ridges in contour represent material lines of exponential stretching when

integrated forward in time. In other words, a pair of particles straddled along a ridge of iFTLE are exponentially apart at $t = 15$. It is noteworthy that particle positions vary widely with increase in St between fig. 3.5 (a), & (c). Despite the above fact iFTLE, a measure derived from particle positions exhibits no significant change between fig. 3.5 (d), (e) & (f). As a consequence, a pair of particles straddled along a ridge in fig. 3.5 (f) are most likely to be found in different attractors of fig. 3.5 (c) at $t = 15$, while a similar pair of particles initially straddled along a ridge from fig. 3.5 (d) are less constrained in their phase space as seen in fig. 3.5 (a). This also indicates that increasing St has a significant effect on particle trajectories in our specific flow while having very little on the organizing structure of the flow, the LCS. Based on these observations it is also possible to devise a strategy to segregate inertial particle by Stokes number. For instance higher St particles can be extracted out of the flow at near vicinity of the attractors. Also the fact that nFTLE of fluid particles act as an skeleton to inertial attractors, will aid in segregating the particles.

iFTLE of inertial particles with various St and R are shown in fig. 3.6. Contours of heavy particles, $R = 0$ are shown in the first column while the second and the third columns represent iFTLE of neutrally buoyant and light particles, respectively. Increasing St for heavy particles ($R = 0$) leads to more ridges as shown. On the other hand increasing St for bubbles ($R = 1$) lead to relatively fewer ridges of iFTLE, i.e., comparing fig. 3.6 (m) & (o) it is clear that increasing St leads to relatively more and less ridges, respectively, in the cell $[0, 2]$ x $[0, 1]$. Since iFTLE are measures of exponential stretching of material lines they can be construed as an indicator of mixing between particles. In light of the above, it is clear that increasing St leads to relatively better mixing for aerosols ($R = 0$) while the contrary is true for bubbles. This result emphasizes the fact that optimum mixing occurs at different St for bubbles and aerosols.

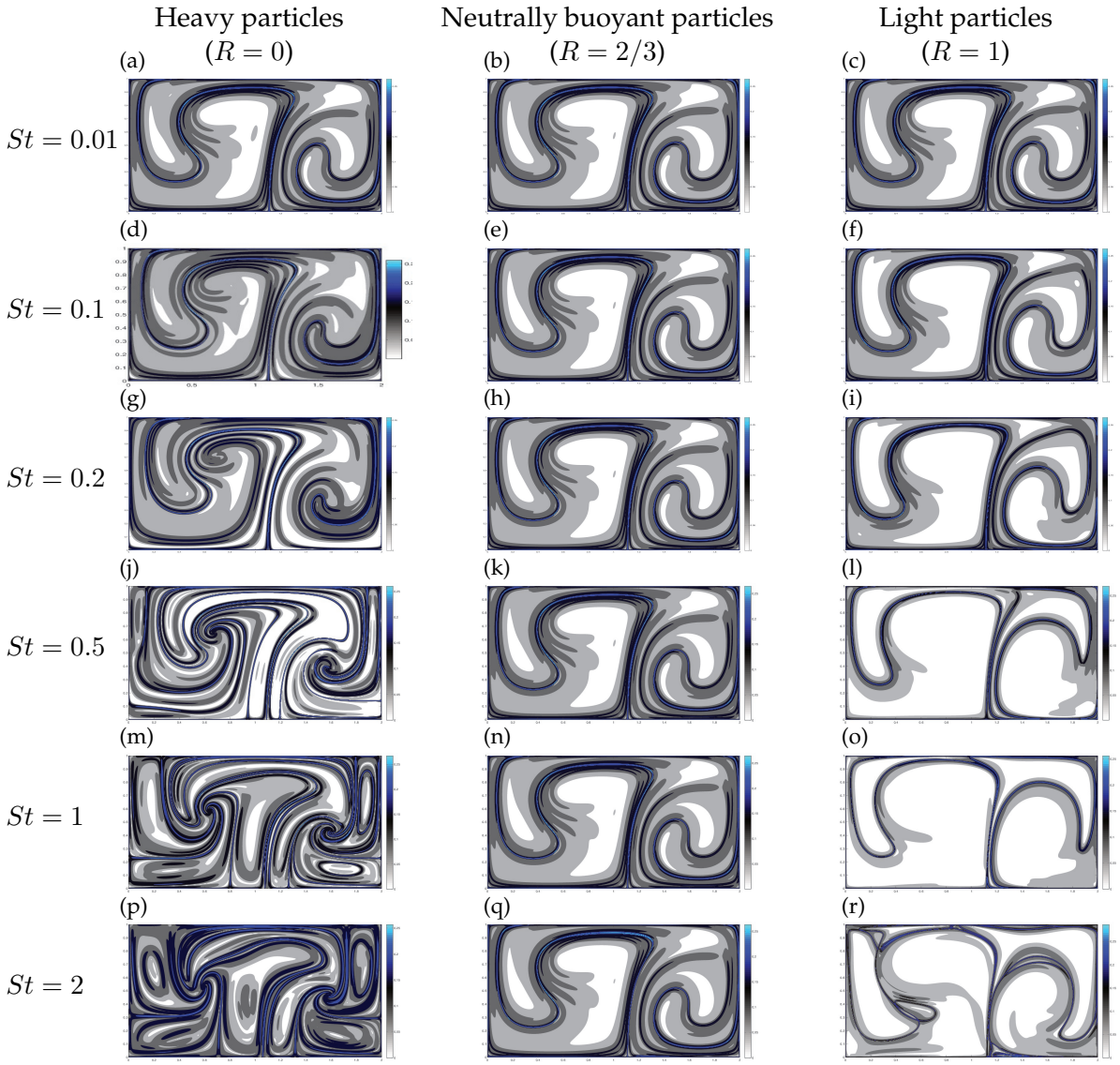

Figure 3.6: pFTLE for inertial particles with St ranging from 0.01 to 2 and R from 0 to 1 with $\omega = \frac{2\pi}{10}$.

3.3 Dispersion and mixing of inertial particles

Figure 3.7 compares contour plots of single point dispersion, D_1, two point dispersion, D_2 and inertial finite-time Lyapunov exponents evaluated for particles with $R = 1$ and

$St = 0.5$. For instance, Figure 3.7 (a) plots the well know single point dispersion, D_1 for each particle as defined below in a contour plot.

$$D_1(t) = \frac{1}{N} \sum_{all\ particles} ||\overrightarrow{r_1}(0) - \overrightarrow{r_1}(t)||, \tag{3.4a}$$

$$D_2(t) = \frac{1}{4(N-1)} \sum_{i\ over\ 4\ neighboring\ particles} ||\overrightarrow{r}_1(t) - \overrightarrow{r}_i(t)||, \tag{3.4b}$$

here $\overrightarrow{r_1}(t) = (x_1,\ y_1)$ represents the position of particle under consideration at time t and N denotes the total number of particles.

In accordance with the equations above, dispersion is defined as the standard deviation of the distribution of particle pair distances. In eq. 3.4b each neighboring particles refers to the four immediate neighboring particles from the initial uniform arrangement of particles. From the above definitions D_1, single point dispersion, is a measure of how far the particles have traversed from their original position while D_2, two-point dispersion measures relative separation between neighboring particles. In contrast to our definition, Waugh et al. [2012] analyzed a measure analogous to D_2, but their work computes particle separations between all possible pairs of particles. They showed the analytical relationship between FTLE, D_2 and a closely related quantity finite size Lyapunov exponents (FSLEs). We numerically extend these results for inertial particles by demonstrating similarities between two-point dispersion, D_2 and iFTLEs. The above result is of great interest since it hints at a possible theoretical connection between dispersion, a well studied measure in fluid dynamics, and finite time Lyapunov exponents. Another consequence of our finding is that material surfaces identified by iFTLEs are the ones that are maximally dispersed through the flow.

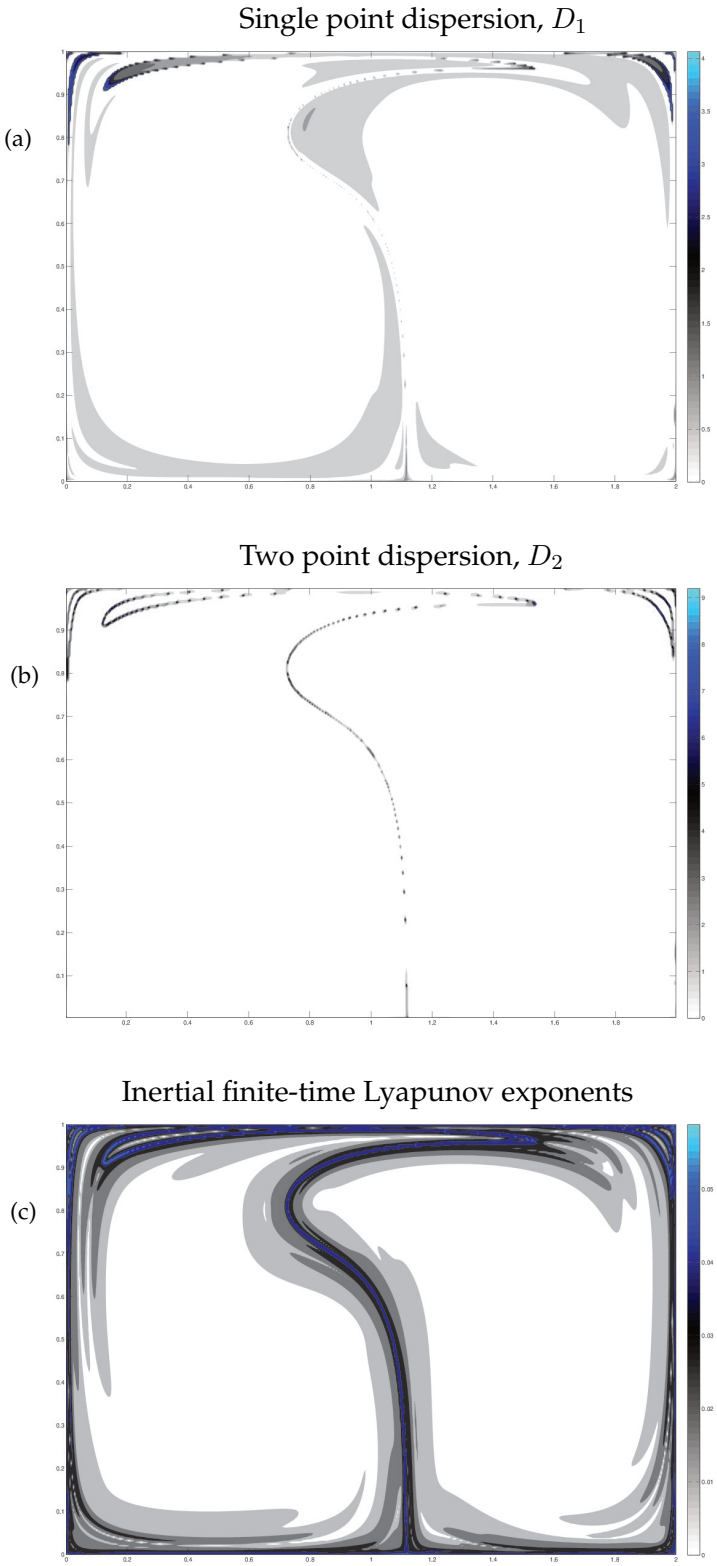

Figure 3.7: Single point dispersion, D_1, two point dispersion, D_2 and inertial finite time Lyapunov exponents of particle trajectories at $t = 15$ for $\omega = \frac{6\pi}{10}$, $R = 1$ and $St = 0.5$.

Chapter 4

CONCLUSIONS AND FUTURE WORK

4.1 Concluding remarks

In this work, an attempt to interpret the characteristics of inertial particles through computing Finite time Lyapunov exponents, has been made. Distinctions based on parameters St, R of the particles and ω, the corresponding frequency of the flow have been discussed with the help of iFTLE (inertial Finite time Lyapunov exponents), single point and two-point dispersion statistics.

Dynamics of inertial particles were found to be monotonically dissipative as opposed to non-inertial flows where the phase space (x, y) is preserved. We assumed a periodic stream-function, known as the double gyre to numerically illustrate this phenomenon. Stokes number, St, the non-dimensional particle response time to flow was increased to demonstrate higher rates of dissipation resulting in increasingly thinner structures. These effects were existent irrespective of the density of particles. A comparison of these effects on both aerosols and bubbles was drawn by altering R, the non-dimensional density parameter.

It is numerically shown that with $R = \frac{2}{3}$, the neutrally buoyant particles initiated with local flow velocity $v(0) = u(0)$, follow the corresponding fluid particles, i.e., $v(t) = u(t)$. On the other hand the value of the non dimensional density parameter, R had a significant effect on both aerosol and bubble particle trajectories. In fact inertial particles are seen preferentially concentrating on specific regions of the flow depending on R. This is because aerosols experience more centrifugal force pushing them out of vorticity centers while bubbles are under the influence of stronger pressure gradient forces driving them radially inwards towards low vorticity, high rate of strain regions. These effects are shown

to be more pronounced with increase in St, since increasing St leads to higher dissipation rate of phase space, ($x,\ y$).

Furthermore, increasing ω, the flow frequency emphasizes the filtering effect of St on particle response. Remarkable similarities between the trajectories of particles on a steady ($\omega = 0$) and high frequency ($\omega = 10$) flows have been observed in accord with the attenuating effect of St on flow frequency. Although such effects have been observed by Bec et al. [2006], our results extend these observations to bubbles whose densities are less than the base fluid.

Inertial Finite time Lyapunov exponents (iFTLE) were evaluated on particle trajectories and were used to provide supplementary information in interpreting the dynamics. The main result is that inertial particles were observed to be attracted/repelled from the attractive manifolds (nFTLE) of the fluids. This result supplements other well-known results of preferential concentration. Our results indicate that nFTLE of the underlying fluid system acts as an skeleton in organizing the inertial particles. Consequently nFTLE are more accurate in pinpointing zones of preferential concentration of inertial particles. Based on our results we propose applying inertial particles in identifying coherent features of the flow.

Increasing St of particles leads to relatively higher rate of phase space dissipation. However iFTLE contours of the corresponding system retain most significant ridges as St is increased. In addition magnitude of the ridges are comparable to each other. Therefore a scenario with very similar iFTLE contours with dissimilar particle trajectories is reported. Taking into account the attractors formed by higher St particles, the above fact implies that higher St particles straddled along a ridge of iFTLE are most likely to be entrained into different attractors while relatively lower St particles are observed to fill most of the phase space. This result is suggested to have implications on techniques to segregate inertial particle by Stokes number.

Inertial finite-time Lyapunov exponents being measures of exponential stretching can

be construed as an indicator of mixing of inertial particles. Considering this fact increasing St for bubbles results in qualitatively fewer ridges indicating poor mixing between them. On the other hand increasing St has a contradictory effect on aerosols with noticeably more ridges, indicating better mixing. The above findings suggest that optimum mixing occurs at different St for bubbles and aerosols.

Furthermore, qualitative similarities are shown between the well studied two-point dispersion and iFTLE. Two point dispersion evaluated on the inertial particles shows close similarities with dominant ridges of iFTLE. We numerically extend the results of Waugh et al. [2012] for inertial particles.

4.2 Future work

The current work relied on a simple two dimensional planar stream-function generated flow in illustrating the use of iFTLE. Consequently a natural extension would be to examine these effects on 3D flows. This is especially beneficial since most flows in nature and industrial process are 3D. In section 3.2 our results indicated that increasing St retains the dominant ridges of iFTLE. In light of this finding, devising a control strategy to segregate particles based on St can be a future possibility. Furthermore, based on the fact that inertial particles are attracted onto the nFTLE of the fluid system, it is suggested that inertial flow visualization can be employed to visualize these structures in experiments.

Results from section 3.3 suggest that particles straddled along a ridge of iFTLE get dispersed throughout the flow because of the fact that dominant ridges of iFTLE coincide with those from D_2, a two-point dispersion measure. Therefore these locations become a natural choice for initiating particles in flow visualization studies. Conducting experimental studies along these lines is another future possibility. In addition our finding that material surfaces identified by iFTLE ridges being the most dispersed surfaces of flow has significant applications in designing chemically reactive process, especially non premixed

combustion processes. For instance designing the interface between oxidant and fuel to align with a ridge of iFTLE is expected to increase the rate of reaction. This is ascribed to our finding that iFTLE ridges are maximally dispersed[1], as a result the interfacial length is expected to be optimized thereby mixing oxidant and fuel molecules well. However as pointed out earlier, these results were obtained assuming a planar two dimensional flow. In this regard, a carefully study modeling the effect of 3D turbulence and accurate reaction kinetics is essential in establishing the aforesaid hypothesis.

[1]IFTLE ridges were found to coincide well with those from D_2, a two-point dispersion measure.

BIBLIOGRAPHY

H. Aref. Stirring by chaotic advection. *Journal of Fluid Mechanics*, 143:1–21, 1984.

A. Babiano, J. H. E. Cartwright, O. Piro, and A. Provenzale. Dynamics of a small neutrally buoyant sphere in a fluid and targeting in Hamiltonian systems. *Physical Review Letters*, 84(25):5764–5767, 2000.

Jeremy Bec, Luca Biferale, Guido Boffetta, Antonio Celani, Massimo Cencini, Alessandra Lanotte, S Musacchio, and Federico Toschi. Acceleration statistics of heavy particles in turbulence. *Journal of Fluid Mechanics*, 550:349–358, 2006.

FJ Beron-Vera, MJ Olascoaga, and GJ Goni. Oceanic mesoscale eddies as revealed by lagrangian coherent structures. *Geophysical Research Letters*, 35(12), 2008.

Luca Biferale, G Boffetta, A Celani, BJ Devenish, A Lanotte, and Federico Toschi. Lagrangian statistics of particle pairs in homogeneous isotropic turbulence. *Physics of Fluids*, 17(11):115101, 2005.

G Boffetta and IM Sokolov. Statistics of two-particle dispersion in two-dimensional turbulence. *Physics of Fluids*, 14(9):3224–3232, 2002.

L Chen, S Goto, and JC Vassilicos. Turbulent clustering of stagnation points and inertial particles. *Journal of Fluid Mechanics*, 553:143–154, 2006.

Clayton T Crowe. *Multiphase flow handbook*. CRC Press, 2005.

John K Eaton and JR Fessler. Preferential concentration of particles by turbulence. *International Journal of Multiphase Flow*, 20:169–209, 1994.

John R Fessler, Jonathan D Kulick, and John K Eaton. Preferential concentration of heavy particles in a turbulent channel flow. *Physics of Fluids*, 6(11):3742–3749, 1994.

JCH Fung and JC Vassilicos. Two-particle dispersion in turbulentlike flows. *Physical Review E*, 57(2):1677–1690, 1998.

MA Green, CW Rowley, and George Haller. Detection of lagrangian coherent structures in three-dimensional turbulence. *Journal of Fluid Mechanics*, 572:111–120, 2007.

G. Haller. Lagrangian coherent structures from approximate velocity data. *Physics of Fluids*, 14(6):1851–1861, June 2002.

G Haller and AC Poje. Finite time transport in aperiodic flows. *Physica D: Nonlinear Phenomena*, 119(3):352–380, 1998.

G. Haller and T. Sapsis. Where do inertial particles go in fluid flows. *Physica D*, 237:573–583, 2008.

G Haller and G Yuan. Lagrangian coherent structures and mixing in two-dimensional turbulence. *Physica D: Nonlinear Phenomena*, 147(3):352–370, 2000.

George Haller. A variational theory of hyperbolic lagrangian coherent structures. *Physica D: Nonlinear Phenomena*, 240(7):574–598, 2011.

JH LaCasce. Statistics from lagrangian observations. *Progress in Oceanography*, 77(1):1–29, 2008.

Nadeem A Malik and JC Vassilicos. A lagrangian model for turbulent dispersion with turbulent-like flow structure: Comparison with direct numerical simulation for two-particle statistics. *Physics of Fluids*, 11(6):1572–1580, 1999.

M. R. Maxey and J. J. Riley. Equation of motion for a small rigid sphere in a nonuniform flow. *Physics of Fluids*, 26:883–889, 1983.

MR Maxey. The gravitational settling of aerosol particles in homogeneous turbulence and random flow fields. *Journal of Fluid Mechanics*, 174:441–465, 1987a.

MR Maxey. The motion of small spherical particles in a cellular flow field. *Physics of Fluids (1958-1988)*, 30(7):1915–1928, 1987b.

MR Maxey and S Corrsin. Gravitational settling of aerosol particles in randomly oriented cellular flow fields. *Journal of the atmospheric sciences*, 43(11):1112–1134, 1986.

Igor Mezić, S Loire, Vladimir A Fonoberov, and P Hogan. A new mixing diagnostic and gulf oil spill movement. *Science*, 330(6003):486–489, 2010.

EE Michaelides. Reviewthe transient equation of motion for particles, bubbles, and droplets. *Journal of fluids engineering*, 119(2):233–247, 1997.

DFS Natusch, JR Wallace, and CA Evans. Toxic trace elements: preferential concentration in respirable particles. *Science*, 183(4121):202–204, 1974.

Francesco Nencioli, Francesco d'Ovidio, AM Doglioli, and AA Petrenko. Surface coastal circulation patterns by in-situ detection of lagrangian coherent structures. *Geophysical Research Letters*, 38(17), 2011.

María J Olascoaga and George Haller. Forecasting sudden changes in environmental pollution patterns. *Proceedings of the National Academy of Sciences*, 109(13):4738–4743, 2012.

J. Peng and J. O. Dabiri. Transport of inertial particles by Lagrangian coherent structures: application to predator-prey interaction in jellyfish feeding. *Journal of Fluid Mechanics*, 623:75–84, 2009.

Siméon Denis Poisson. *Mémoire sur les équations générales de l'équilibre et du mouvement des corps solides élastiques et de fluides*. L'imprimerie Royale, 1831.

V Rom-Kedar, A Leonard, and S Wiggins. An analytical study of transport, mixing and chaos in an unsteady vortical flow. *Journal of Fluid Mechanics*, 214:347–394, 1990.

J Rubin, CKRT Jones, and M Maxey. Settling and asymptotic motion of aerosol particles in a cellular flow field. *Journal of Nonlinear Science*, 5(4):337–358, 1995.

Juan PLC Salazar and Lance R Collins. Two-particle dispersion in isotropic turbulent flows. *Annual Review of Fluid Mechanics*, 41:405–432, 2009.

Themistoklis Sapsis and George Haller. Inertial particle dynamics in a hurricane. *Journal of the Atmospheric Sciences*, 66(8), 2009.

Themistoklis Sapsis and George Haller. Clustering criterion for inertial particles in two-dimensional time-periodic and three-dimensional steady flows. *Chaos: An Interdisciplinary Journal of Nonlinear Science*, 20(1):017515, 2010.

S. C. Shadden, F. Lekien, and J. E. Marsden. Definition and properties of Lagrangian coherent structures from finite-time Lyapunov exponents in two-dimensional aperiodic flows. *Physica D*, 212:271–304, 2005.

SC Shadden, K Katija, M Rosenfeld, JE Marsden, and JO Dabiri. Transport and stirring induced by vortex formation. *Journal of Fluid Mechanics*, 593:315–331, 2007.

Shawn C Shadden. Lagrangian coherent structures. *Transport and Mixing in Laminar Flows: From Microfluidics to Oceanic Currents*, pages 59–89, 2005.

Raymond A Shaw, Walter C Reade, Lance R Collins, and Johannes Verlinde. Preferential concentration of cloud droplets by turbulence: Effects on the early evolution of cumulus cloud droplet spectra. *Journal of the atmospheric sciences*, 55(11):1965–1976, 1998.

Kyle D Squires and John K Eaton. Preferential concentration of particles by turbulence. *Physics of Fluids A: Fluid Dynamics (1989-1993)*, 3(5):1169–1178, 1991.

P. Tallapragada and S. D. Ross. Particle segregation by Stokes number for small neutrally buoyant spheres in a fluid. *Physical Review E*, 78:036308–1–036308–9, 2008.

P. Tallapragada, S. D. Ross, and D. G. Schmale III. Lagrangian coherent structures are associated with fluctuations in airborne microbial populations. *Chaos*, 21:033122–1–033122–16, 2011.

W. Tang, B. Knutson, A. Mahalov, and R. Dimitrova. The geometry of inertial particle mixing in urban flows, from deterministic and random displacement models. *Physics of Fluids*, 24:063302–1–063302–18, 2012.

GI Taylor. Diffusion and mass transport in tubes. *Proceedings of the Physical Society. Section B*, 67(12):857, 1954.

Tamás Tél, Alessandro de Moura, Celso Grebogi, and György Károlyi. Chemical and biological activity in open flows: a dynamical system approach. *Physics reports*, 413(2): 91–196, 2005.

N Nirmal Thyagu and Neelima Gupte. Clustering, chaos, and crisis in a bailout embedding map. *Physical Review E*, 76(4):046218, 2007.

Federico Toschi, Jeremie Bec, Luca Biferale, Guido Boffetta, Antonio Celani, Massimo Cencini, Alessandra Lanotte, and Stefano Musacchio. Acceleration statistics of heavy particles in turbulence. In *APS Division of Fluid Dynamics Meeting Abstracts*, volume 1, 2005.

Darryn W Waugh, Shane R Keating, and Mei-Lin Chen. Diagnosing ocean stirring: Comparison of relative dispersion and finite-time lyapunov exponents. *Journal of Physical Oceanography*, 42(7), 2012.

AM Wood, W Hwang, and JK Eaton. Preferential concentration of particles in homogeneous and isotropic turbulence. *International journal of multiphase flow*, 31(10):1220–1230, 2005.

Jigen Zhou, RJ Adrian, S Balachandar, and TM Kendall. Mechanisms for generating coherent packets of hairpin vortices in channel flow. *Journal of Fluid Mechanics*, 387:353–396, 1999.

VITA

Sudharsan Madhavan received his Bachelor of technology (B. Tech.) degree in July 2012 from the department of Mechanical Engineering at Indian Institute of Information Technology (IIIT), Kancheepuram, Chennai, India. At IIIT, he worked under the supervision of Prof. S. Jayavel on flow and heat transfer characteristics of fin-tube heat exchangers. Simultaneously he was also working with Prof. T. Sundararajan and Prof. Shaligram Tiwari on understanding the intriguing dynamics of flow past bluff bodies through novel immersed boundary methods. Additionally he was also designing and building an open circuit wind tunnel along with Dr. Diwakar Venkatesan and S. Ganga Prasath. In September 2012 he joined the Applied Mathematics department at University of Washington, Seattle. He has been working under the supervision of Prof. James Riley and Prof. Steven Brunton on comprehending the fascinating connections between the dynamics of inertial particles and Lagrangian Coherent Structures. He took immense joy in working with such intellectually stimulating and encouraging collaborators. He is looking forward to join the Ira A. Fulton School of Engineering at Arizona State University as a doctoral researcher.